Journal of Materials Chemistry A

Efficient single-atom Ni for catalytic transfer hydrogenation of furfural to furfuryl alcohol

Journal:	*Journal of Materials Chemistry A*
Manuscript ID	TA-ART-11-2020-010838.R2
Article Type:	Paper
Date Submitted by the Author:	03-Dec-2020
Complete List of Authors:	Fan, Yafei; Southwest Forestry University, Zhuang, Changfu; Southwest Forestry University, Li, Shangjing; Southwest Forestry University, Wang, Ying; Southwest Forestry University, Zou, Xiaoqin; Northeast Normal University Liu, Xiaoteng; Northumbria University, Department of Mechanical & Construction Engineering Huang, Weimin; Jilin University, Guangshan, Zhu; Northeast Normal University School of Chemistry, Chemistry

ARTICLE

Efficient single-atom Ni for catalytic transfer hydrogenation of furfural to furfuryl alcohol

Received 00th January 20xx,
Accepted 00th January 20xx

DOI: 10.1039/x0xx00000x

Yafei Fan,[a] Changfu Zhuang,[a*] Shangjing Li,[a] Ying Wang,[a] Xiaoqin Zou,[b*] Xiaoteng Liu,[c*] Weimin Huang[d] and Guangshan Zhu[b]

The employment of single-atom catalysts in the catalytic transfer hydrogenation (CTH) of furfural (FF) to furfuryl alcohol (FAL) have never been effectively explored. Herein, Ni single-atoms supported on nitrogen doped carbon (Ni-SAs/NC) catalyst is synthesized and first ever utilized in CTH of FF to FAL. Atomically dispersed Ni-N_4 sites change the electron density at the metal center and exhibit specific adsorption and desorption to FF and FAL, promoting an outstanding catalytic performance with turnover frequency (TOF) of 832 h^{-1} and selectivity as high as 97.1% at 130 °C for 2 h. Such performance is 9-fold higher than that of supported Ni nanocatalysts. The Ni-SAs/NC catalyst also exhibits superior stability for CTH of FF and excellent catalytic activity for other α,β-unsaturated aldehydes. This work provides a new strategy of producing green chemical compounds using catalytic biomass conversion and suggests the future application of long-lasting single-atom catalysts for emerging sustainable technologies.

1. Introduction

Selective conversion of biomass resources to biofuels and platform molecules has attracted extensive attention for chemical production industry.[1-5] Furfural (FF), as a versatile biomass-derived platform compound, serving as a precursor to produce over 80 different industrial chemicals, owing to the presence of C=O and C=C bonds.[6-9] Furfuryl alcohol (FAL) is an important hydrogenation product of FF and it is widely used in synthetic resins, reactive solvent and production of chemicals.[10-12] Traditional biorefinery of FF to produce furfuryl alcohol (FAL) is constrained by high pollution and toxicity, low selectivity and high-cost *etc*., which made this process not economically and environmentally viable.[13] In addition, high-pressure reaction with H_2 as H-donor has many drawbacks, such as highly flammable, explosive and high instrumental requirements.[14-15] Advantages over H_2 as H-donor, catalytic transfer hydrogenation (CTH) has received increasing attention, due to it uses low cost and readily available alcohol compounds as H-donor , so CTH offers a greener, more effective and safer hydrogenation reaction process.[16-19]

A variety of noble catalysts have been studied for CTH reactions of FF, including Pt[20], Pd[21], Ru[22] etc. High catalytic activity has been received using noble metal catalysts, but it often accompanied with side reactions of over hydrogenation resulting in low selectivity. Outstanding performance for hydrogen dissociation has been achieved using low-cost non-noble Ni-based catalysts for selective hydrogenation of FF,[23-24] but the main problem is the low transformation efficiency, and Ni species tend to leach and aggregate in the reaction process.[25] Therefore, development of efficient and stable Ni-based catalysts for CTH of FF to FAL has become the research challenge.

Single-atom catalysts (SACs) have been revealed for their advanced performance towards multiple catalytic reactions.[26-29] Unlike conventional metal nanoparticles (NPs) catalysts, isolated metal atoms supported on substrate materials display unique features, *i.e.* maximized exposure of the active sites, ultra-uniform distribution, quantum size effect, altered atom-substrate interaction, unsaturated coordination configuration etc.[30-32] SACs derived from zeolite imidazolate frameworks (ZIFs) are emerging investigations, which have demonstrated good catalytic activity and selectivity in the electrocatalysis[33], photocatalysis[34] and thermocatalytic.[35] When ZIFs precursor is pyrolyzed, the evaporation of zinc at high temperature can prevent metal atoms from agglomerating to obtain stable SACs.[36] Nitrogen doping can also regulate the nanostructure and coordination bonds of metal sites and improve the thermal stability of metal atoms.[37-38] The metal atoms are anchored on the N-doped carbon to form the M-N_x structure after pyrolysis and different coordination structure can induce the change of electronic structure at the active site of the metal, leading to the difference of catalytic activity and

[a] *Key Laboratory of Forest Resources Conservation and Utilization in the Southwest Mountains of China Ministry of Education, School of Chemical Engineering, Southwest Forestry University, Kunming 650051, P. R. China. Email: cfzhuang@swfu.edu.cn.*
[b] *Faculty of Chemistry, Northeast Normal University, Changchun 130024, P. R. China. E-mail: zouxq100@nenu.edu.cn.*
[c] *Department of Mechanical and Construction Engineering, Faculty of Engineering and Environment, Northumbria University, Newcastle upon Tyne, NE1 8ST, United Kingdom. Email: terence.liu@northumbria.ac.uk*
[d] *College of Chemistry, Jilin University, Changchun 130012, P. R. China.*
Electronic Supplementary Information (ESI) available: [details of any supplementary information available should be included here]. See DOI: 10.1039/x0xx00000x

selectivity.[39-40] In addition, ZIFs derived SACs have excellent pore structure, which can effectively promote the transport of reactants and improve the catalytic performance.[41] Nevertheless, SACs derived from ZIFs have never been effectively explored in CTH of FF to FAL.

Herein, we report Ni single-atoms supported on N-doped porous carbon (Ni-SAs/NC) catalyst, which was first ever utilized in CTH of FF to FAL. The catalyst exhibits an excellent activity for CTH of FF with TOF is as high as 832 h^{-1} and selectivity is 97.1% for hydrogenation of FF, and this catalyst significantly improved catalytic performance for 9 times than Ni nanoparticles/N-doped porous carbon (Ni-NPs/NC). The mechanism of this reaction was investigated in detail, including solvent, reaction time and temperature. In addition, Ni-SAs/NC exhibits good stability of FF hydrogenation for four cycles of reuse.

2. Experimental

2.1 Synthesis of Ni@ZIF-8

An encapsulation method was used to prepare Ni@ZIF8. Brief details include 2-methylimidazole (16 mmol) was dissolved in 15 mL methanol with stirring in flask A. $Zn(NO_3)_2{\cdot}6H_2O$ (4 mmol) and $Ni(acac)_2{\cdot}2H_2O$ (0.4 mmol) were dissolved in 30 mL methanol under ultrasonic mixing for 15 min to form a clear solution in flask B. Then, flask A was subsequently added into flask B with vigorous stirring for 1 h at room temperature. The solution was transferred into a 100 mL Teflon lined stainless-steel autoclave and heated at 120 °C for 4 h. The obtained product was separated by centrifugation and washed subsequently with CH_3OH for third and finally dried at 70 °C under vacuum for overnight. For the purpose of synthesis Ni-NPs/NC, we also synthesized 5Ni@ZIF-8 using the same procedure, but the extra 2 mmol of $Ni(acac)_2$ and 4 mmol $Zn(NO_3)_2{\cdot}6H_2O$ were dissolved in 30 mL methanol under ultrasonic mixing for 15 min to form a clear solution in flask B.

2.2 Synthesis of Ni-SAs/NC

The powder of Ni@ZIF-8 was transferred into a crucible boat and placed in a tube furnace. The sample was heated to 900 °C with a heating rate of 5 °C min^{-1} and kept at 900 °C for 2 h under argon gas flow and then cooled to room temperature. The obtained material was directly used without further treatment. NC and Ni-NPs/NC are synthesized in the same way with Ni-SAs/NC, and their precursor is ZIF-8 and 5Ni/ZIF-8, respectively. Ni/NC and Ni/AC were synthesized by impregnation with NC and activated carbon (AC) as carriers. A schematic diagram shows the whole preparation procedure is illustrated in Figure 1a.

2.3 Characterization

Powder X-ray diffraction (XRD) patterns were analyzed using a Rigaku Ultima X-ray diffraction spectrometer with Cu Kα radiation (λ = 1.5418 Å) at 40 kV and 40 mA. Brunauer-Emmet-Teller (BET) specific area and pore size distribution of the catalysts was characterized by N_2 adsorption-desorption measurement at 77 K using ASAP 2020 Plus Physisorption instrument. XPS analysis was performed on a PHI5000 Versa probe-II Scanning XPS Microprobe system. The morphology of the catalyst was researched using a scanning electron microscope (SEM, Hitachi SU8010). Abbreviated correction Transmission electron microscopy (TEM) images were obtained with a JEM-2100 working at 200 kV. The high-angle annular dark-field scanning transmission electron microscopy (HAADF-STEM) images were imaged by using a FEI Themis Z at 300 kV, equipped with a probe spherical aberration corrector. The X-ray absorption fine structure spectra (Ni K-edge) were collected at 1W1B station in Beijing Synchrotron Radiation Facility (BSRF). The storage rings of BSRF were operated at 1.5 GeV with a maximum current of 200 mA. The metal contents in the samples were measured by the inductively coupled plasma optical emission spectrometry (ICP-OES) using a VISTA-MPX instrument.

2.4 Catalysis Evaluation

The catalytic hydrogenation performance of FF was measured in a 25 mL autoclave reactor with a reaction solution of 1 mmol of FF, 25 mg of catalyst, and 8 mL of 2-propyl alcohol (2-ProOH). The reactor was purged three times with N_2 and pressurized with 2 MPa N_2, and then the reactor was heated to the set temperature of 120 °C while being magnetically stirred at a rate of 800 rpm. At the end of the reaction, the liquid samples were collected for analysis. The used catalyst was filtered, washed with ethanol and then dried at 80 °C in vacuum. Then the catalysts are reduced at 400 °C with 10% H_2/Ar for further reactions and characterizations.

The liquid products were diluted in methanol then analyzed using gas chromatography-mass spectrometry (GC-MS, QP2010 SE, Shimadzu) and quantitatively analyzed using GC (GC-7890A, Agilent), equipped with FID and a (30 m × 0.25 mm × 0.25 μm) KB-WAX capillary column (Kromat Corporation, USA). 1.0 uL sample was injected into the injection port with a split ratio of 30:1. The column temperature was initially maintained at 40 °C for 1 min followed by heating up to 220 °C at a ramp rate of 20 °C/min and the temperature was held at 250 °C for 1 min using nitrogen as the carrier gas.

The conversion of reactant is defined with the following equation:

$$\text{Conversion}\ (\%) = \frac{\text{Mole of FF converted}}{\text{Mole of FF loaded}} \times 100\%$$

The selectivity of product is defined with the following equation:

$$\text{Selectivity}\ (\%) = \frac{\text{Mole of FAL produced}}{\text{Mole of product produced}} \times 100\%$$

3. Results and discussion

XRD was used to determine the structural information of the catalyst. Figure 1b shows the XRD patterns of the Ni@ZIF-8 and 5Ni@ZIF-8, which were matched with ZIF-8. Ni-SAs/NC shows a peak located around 26° corresponding to the (002) plane of graphite carbon, which was the same as that of Ni-NPs/NC and NC in Figure 1c. Ni-NPs/NC did not show the characteristic diffraction peak of Ni due to its relatively low Ni content and single Ni atoms could be under the detection limit

of the technique. Table S1 listed the pore structure data and metal content of materials. BET surface area measurement was used to determine the catalysts. The N_2 adsorption/desorption isotherm indicates that the content of Ni had an important effect on the structure of porous carbon. In Figure 1d, all samples follow type-IV isotherms, indicating that the micro-mesoporous co-exist in the porous carbon. Compared to precursor Ni@ZIF-8 (1910 m^2 g^{-1}), the specific surface area of Ni-SAs/NC (1037 m^2 g^{-1}) was significantly reduced. During the pyrolysis process, the pore structure of the precursor partially collapsed, resulting in a significant decrease in the specific surface area of the derived Ni catalyst. As the Ni contents increase, more Ni is confined in the pore structure, so the BET surface area gradually decreased from 1183 m^2 g^{-1} (NC) to 1037 m^2 g^{-1} (Ni-SAs/NC) and 954 m^2 g^{-1} (Ni-NPs/NC). A similar change in the pore volume 0.37 (NC), 0.32 (Ni-SAs/NC) and 0.31 (Ni-NPs/NC) cm^3 g^{-1} was also observed. Figure 1e shows the pore size distribution of the material. Interestingly, Ni-SAs/NC showed the maximum average pore size (2.07 nm) compared with NC (1.79 nm) and Ni-NPs/NC (1.87 nm), which also contribute to the transfer of substrates and products during catalysis.

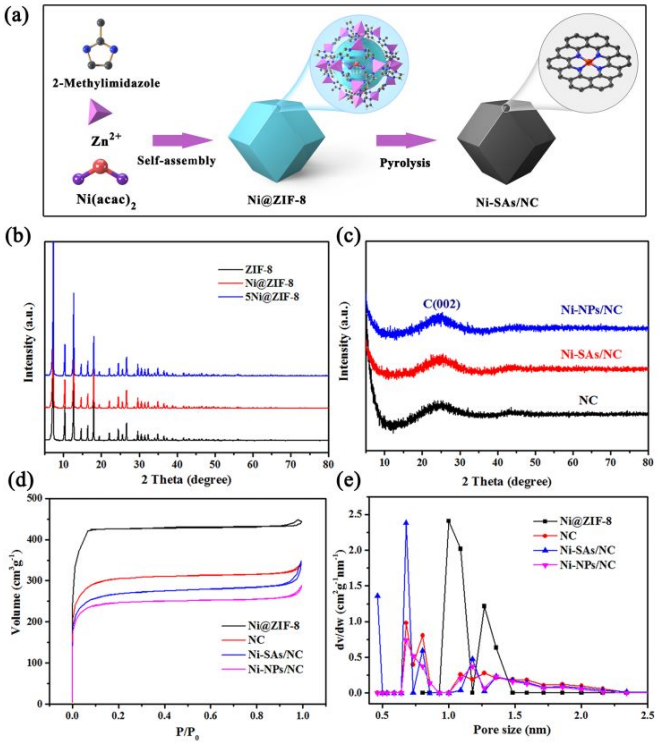

Figure 1. (a) Schematic illustration for the preparation of Ni-SAs/NC catalyst. (b) XRD patterns of precursors. (c) XRD patterns of NC, Ni-SAs/NC and Ni-NPs/NC. (d) N_2 sorption isotherms for Ni@ZIF-8, NC, Ni-SAs/NC and Ni-NPs/NC samples. (e) Pore size distribution.

The morphology of Ni-SAs/NC was observed by SEM and TEM. In Figure 2a-b, Ni-SAs/NC retained the dodecahedral structure of the precursor Ni@ZIF-8 (Figure S1), but the surface became rougher after pyrolysis. However, no particles were observed in the HR-TEM of Ni-SAs/NC (Figure S3). High-angle annular dark-field scanning TEM (HAADF-STEM) elemental mappings clearly showed C, N and Ni uniformly distributed throughout the particles (Figure 2c). The Ni loading was 0.12 wt% in Ni-SAs/NC, according to the ICP-OES analysis. In Figure 2d, Ni single-atoms were clearly observed as isolated bright dots, marked in red circles in the Spherical Aberration Corrected Transmission Electron Microscope (AC-TEM) image. The above results indicate that the Ni was loaded on the N-doped carbon as single atoms. In addition, the morphology of Ni-NPs/NC was severely damaged in Figure S4. The Ni nanoparticles of Ni- NPs/NC were observed on the HR-TEM (Figure S5). Meanwhile, Figure S6 TEM images revealed that Ni nanoparticles of Ni/NC and Ni/AC were uniformly loaded on the NC and activated carbon with a mean size of 4.9 and 6.4 nm, respectively.

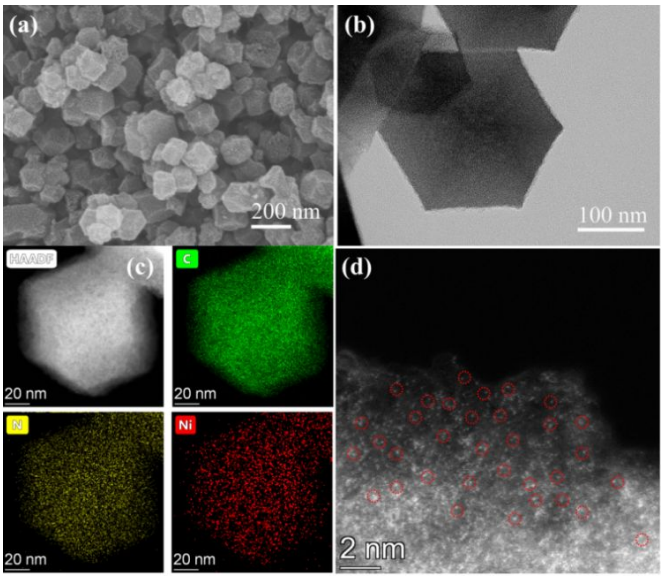

Figure 2. (a) SEM image of Ni-SAs/NC. (b) TEM image of Ni-SAs/NC. (c) HAADF-STEM images of Ni-SAs/NC and corresponding element maps showing the distribution of C (green), N (yellow), Ni(red). (d) AC-TEM images of Ni-SAs/NC. Single Ni atoms highlighted by red circles.

X-ray photoelectron spectroscopy (XPS) was conducted to investigate the elemental composition and valence states in Ni-SAs/NC. The XPS element analysis of the samples is shown in Table S2. In Figure S7d, the XPS results indicated the presence of C, N, O and Ni for Ni-SAs/NC. The Ni-SAs/NC included three main peaks located at 284.6 eV (C=C), 285.8 eV (C=N) and 288.9 eV (C-C) in the one of C 1s.[42] The high-resolution XPS spectra of N 1s revealed the pyridinic-N (398.7 eV), Ni-N (399.2 eV), pyrrolic-N (399.4 eV), graphitic-N (401.0 eV) and oxide-N (403.4 eV) in Figure S7f. Part of the nitrogen in the pyridine-N will coordinate with Ni to form Ni-N (399.2 eV).[43] The advantage of pyridine N can be coordinated with metal atom and used as anchor points to more effectively stabilize the atomically dispersed nickel sites.[44] In Figure S8, the pyridinic-N binding energy of NC was 398.3 eV and 0.4 eV less binding energy relative to Ni-SAs/NC. We think that electron transfer occurs at the coordination of Ni and pyridine-N, caused an increase in the electron density at the center of the Ni.[45] In order to further study the chemical state and

coordination structure of Ni species in Ni-SAs/NC, XANES and EXAFS spectroscopy were performed and results are shown in Figure 3. As we can see from the XANES spectrum (Figure 3a), the Ni-SAs/NC near edge absorption energy is located between NiO and Ni foil, indicating that the valence state of Ni was between 0 and +2, and atomically dispersed Ni is loaded on the NC. EXAFS exhibited that Ni-SAs/NC had a major peak at ~1.31 Å, which is smaller than the Ni-Ni peak at ~2.15 Å for the Ni foil and Ni-O peak at ~1.56 Å for the NiO. This could be due to a mixture of Ni-N and Ni-O bonding, indicating atomic dispersion of the Ni species. Furthermore, EXAFS wavelet transform analysis further revealed the atomic distribution of Ni-SAs/NC. From the Figure 3d-f, Ni foil and NiO standards indicated that the intensity maxima at ~7.9 and ~7.2 $Å^{-1}$. Notably, Ni-SAs/NC exhibited the intensity maximum at ~5.2 $Å^{-1}$, shows Ni atoms are in the form of coordination which associated with the Ni-N(O), this also confirmed the major peak at ~1.31 Å attributes to Ni-N(O) bond (Figure 3b). In addition, least-squares EXAFS curve-fitting analysis was performed to obtain quantitative structural data. The best fitting analysis of Ni-SAs/NC showed the coordination number of Ni is 4.46 and the mean bond length is 1.98 Å (Figure 3c, Figure S10 and Table S3). Above evidence indicates Ni presents as isolated single atom state, and was anchored in a N-doped porous carbon and the Ni atoms and N atoms exist in the form of quaternary coordination ($Ni-N_4$). The atomic structure model was shown in Figure 3c (inset) and O_2 molecules were thought to attach to Ni atoms. The best-fit results of Ni foil and NiO were shown in Figure S9, respectively.

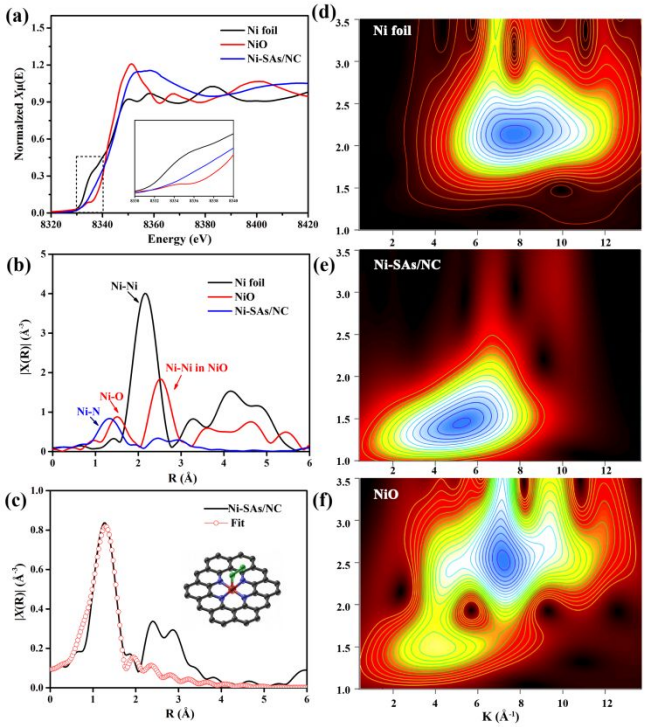

Figure 3. (a) XANES spectra. (b) Fourier transform (FT) of the Ni K-edge EXAFS. (c) EXAFS fitting curve for Ni-SAs/NC samples (inset schematic model of Ni-SAs/NC). (d) Wavelet transform (WT) of Ni foil. (e) Wavelet transform (WT) of Ni-SAs/NC. (f) Wavelet transform (WT) of NiO.

3.2 Catalytic Performance

Table 1. Catalytic transfer hydrogenation of furfural with various catalysts.[a]

Entry	Catalyst	Conv. (%)	Sel. (%)	TOF[b] (h^{-1})	R_{rate}[c] (mmol g^{-1} h^{-1})
1	Blank	0	0	-	-
2	NC	6.3	93.6	-	0.84
3	Ni-SAs/NC[d]	85.1	97.1	832	17.02
4	Ni-SAs/NC	95.6	96.8	623	12.75
5	Ni-NPs/NC	57.2	95.1	69	7.63
6	5% Ni/NC	89.9	96.4	16	11.98
7	5% Ni/AC	21.8	71.5	3.3	2.91
8	5% Pd/C	12.7	0	-	1.69
9	10% Pt/C	19.1	0	-	2.55
10	M-MOF-808[e]	99.2	93.6	17.6	-
11	Zr-LS[f]	92.2	99.4	4.2	9.16
12	NiO(P)-300[g]	72.6	96.7	2.6	3.51
13	BZC[h]	97.8	98.9	0.37	-
14	$Cu/SO_3^{2-}/C$[i]	100	99	0.2	-

[a] Reaction conditions: 1 mmol FF, 8 mL 2-ProOH, 25 mg catalyst, 130 °C, 3 h, 2 MPa N_2. [b] TOF = (converted moles of FF)/(moles of active sites × time). [c] R_{rate} = mmol (converted FF) / [g (catalyst amount) × h (time)]. [d] 130 °C, 2 h. [e] From ref 18. [f] From ref 11. [g] From ref 49. [h] From ref 50. [i] From ref 14.

Table 1 shows the catalytic properties of FF hydrogenation to FAL of NC (Entry 2), Ni-SAs/NC (Entry 3, 4), Ni-NPs/NC (Entry 5), Ni/NC and Ni/AC (Entry 6, 7), together with several catalysts prepared by other researchers as comparison. A reaction without catalyst was performance (Table 1, Entry 1) and it can be noticed that there is no FF was converted into FAL. NC had a conversion rate of 6.3% and selectivity of 93.6% because the doping of nitrogen atoms change the local electron cloud density of delocalized bonds, which leads to the metal catalytic properties (Entry 2).[46] The catalytic activity of the Ni-SAs/NC was carried out for CTH of FF under different reaction time (Entry 3, 4). Ni-SAs/NC exhibited 85.1% conversion when the reaction time at 2 h and the TOF reached an astonishing 832 h^{-1}. This is because atomically dispersed $Ni-N_4$ sites may change the electron cloud density at the metal center and exhibit specific adsorption and desorption to FF and FAL, promoting efficient hydrogen transfer.[47-48] The ultra-high atom utilization has provided maximised active sites, which could improve the reaction efficiency to the highest level. Meanwhile the excellent pore structure of Ni-SAs/NC (1037 m^2 g^{-1}) leads to a significant exposure of Ni monatomic active sites, such pore size (2.07 nm) is greatly beneficial to the mass transfer between substrates and products. Ni-SAs/NC exhibited 95.6% conversion and 96.8% selectivity when the reaction time increased to 3 h. While the selectivity of FAL decreased slightly with the extension of reaction time, this is due to etherification between FF and the solvent. As a comparison, the catalytic performance of Ni nanoparticles on N-doped carbon (Ni-NPs/NC) was also studied. The conversion rate of 57.2% and selectivity of 95.1% were shown over Ni-NPs/NC in 130 °C (Entry 5). The Ni in the Ni-NPs/NC was mainly

in the form of Ni nanoparticles and Ni load was 0.65 wt% (Table S1), which resulting in low atomic utilization. In addition, it confirmed the results from XPS analysis which revealed a lack of clear Ni-N_4 active sites for Ni-NPs/NC. Compared to 1037 m^2 g^{-1} and 2.07 nm Ni-SAs/NC, the specific surface area and pore size of Ni-NPs/NC are as low as 954 m^2 g^{-1} and 1.87 nm, which led to less exposure of catalytic active sites and the release of hydrogenated products. Therefore, Ni-NPs/NC has lower catalytic activity and the TOF was only 69 h^{-1}, which is 1/9 of that of the single-atom Ni-SAs/NC catalyst. Although the metal loading of the Ni-NPs/NC is 5.4 times that of the Ni-SAs/NC, but the conversion rate (R_{rate}) of Ni-SAs/NC catalyst is 1.7 times that of Ni-NPs/NC catalyst. In order to better illustrate the excellent performance of Ni-SAs/NC, we also synthesized Ni nanocatalysts supported on nitrogen carbon materials (Entry 6). The catalyst is Ni nanoparticles with uniform distribution supported by impregnation method (Ni/NC), it shows 89.9% FF conversion, but the TOF was only 16 h^{-1} (Entry 6), which was 1/39 of that of Ni-SAs/NC. The main reason could be the average particle size is 4.9 nm (Figure S6a), which is significantly larger than single-atom Ni. Activated carbon (AC) was used as the support, and surface area of Ni/AC is 1275 m^2 g^{-1}, which is obviously greater than 954 m^2 g^{-1} of Ni-NPs/NC. Although advanced pore structures facilitated material transfer, the conversion of FF was 25% over Ni/AC and the TOF is as low as 3.3 due to larger nanoparticle sizes (6.4 nm, Figure S6b) result in incomplete exposure of active sites and the lack of nitrogen doping (Entry 6 and 7). In conclusion, it was proved once again that the activity of single-atoms Ni catalyst has much higher catalytic activity towards CTH of FF than other Ni catalysts, it also shows higher performance over commercially available Pd/C and Pt/C catalysts as shown in Entry 8-9 (conversion is only 12.7% and 19.1%, with zero selectivity). Moreover, compared to catalysts previously reported in literatures, Ni-SAs/NC demonstrated excellent TOF and higher catalytic activity under mild conditions for CTH of FF to FAL (Table 1, Entry 10-14 and Table S4).

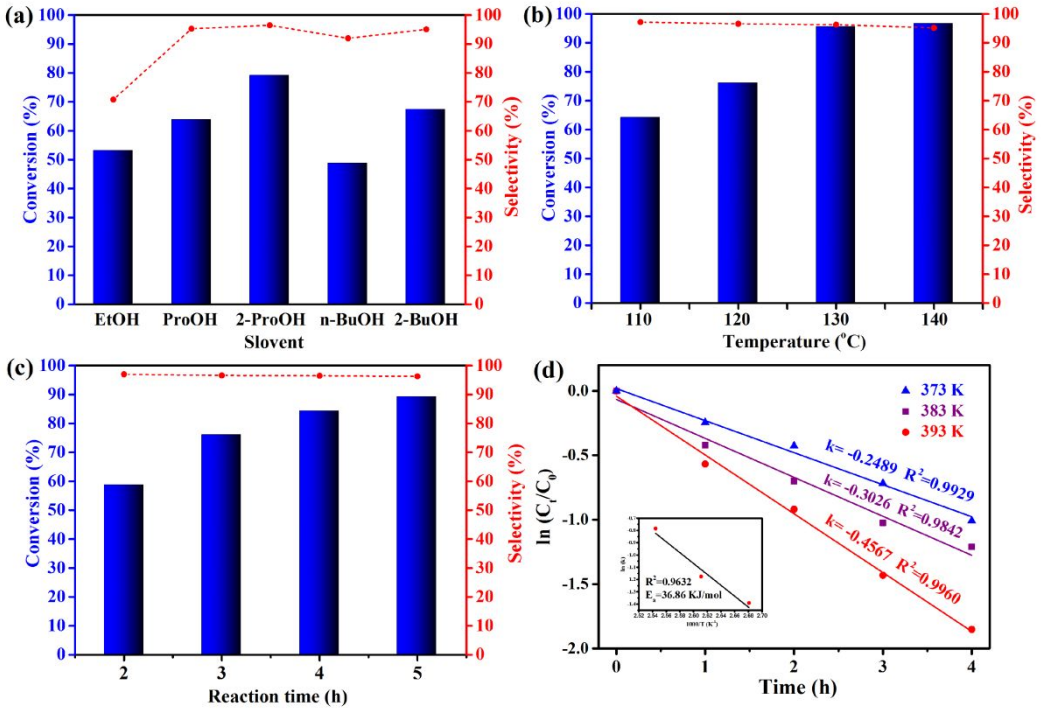

Figure 4. (a) Effect of solvents on hydrogenation of FAL over Ni-SAs/NC. Reaction conditions: 1.0 mmol FF, 25 mg catalyst, 120 °C, 2 MPa N_2, 3 h; (b) Effect of temperature on hydrogenation of FAL over Ni-SAs/NC. Reaction conditions: 1.0 mmol FF, 25 mg catalyst, 8 mL 2-ProOH, 2 MPa N_2, 3 h; (c) Effect of reaction time on hydrogenation of FAL over Ni-SAs/NC. Reaction conditions: 1.0 mmol FF, 25 mg catalyst, 8 mL 2-ProOH, 120 °C, 2 MPa N_2. (d) Kinetic studies of FF hydrogenation over Ni-SAs/NC at different temperatures (the inset represents the Arrhenius plot for the FF hydrogenation). Reaction conditions: 1 mmol FF, 25 mg catalyst, 8 mL 2-ProOH, 2 MPa N_2, 100-130 °C.

3.3. Reaction Mechanism

3.3.1. H-donor Effect

In order to better understand the reaction mechanism of FF hydrogenation to FAL on single-atoms catalyst, a series of catalytic experiments were carried out using Ni-SAs/NC catalysts. Solvent effect plays a very important role in heterogeneous catalysis, so it had a great influence on the activity and selectivity of the catalyst. Therefore, the effect of the H-donor for CTH of FF was researched, including ethanol (EtOH), n-propyl alcohol (PrOH), 2-propyl alcohol (2-ProOH), n-butyl alcohol (n-BuOH) and 2-butyl alcohol (2-BuOH). In Figure 4a, we can see that reaction shows good catalytic activity using alcohols as H-donor. That is because hydrogen bonding between C=O of FF and hydroxyl group of the alcohol contributed to the activation of the FF molecule.[29] When EtOH was used as hydrogen donor, the FF conversion rate was 53.1%

and the selectivity of FAL was 70.8%. Furthermore, secondary alcohols exhibited better catalytic activity than primary alcohols. For example, 2-ProOH had 79.1% conversion and 96.5 selectivity higher than 63.8%, 95.3% of ProOH, and similar results is 67.4% and 95.1% of 2-BuOH better than 48.7%, 92.0% of n-BuOH. β-H on secondary alcohols is more likely prone to β-H elimination than on primary alcohols.[18] In addition, with the increase of the number of carbon in secondary alcohols, the conversion rate of FF decreases obviously. The possible reason for this is that the longer carbon chain of secondary alcohols may lead to a more pronounced negative steric hindrance effect, which prevents FF diffusion in the Ni-SAs/NC channel.[11]

3.3.2. Reaction Temperature and Duration Influence

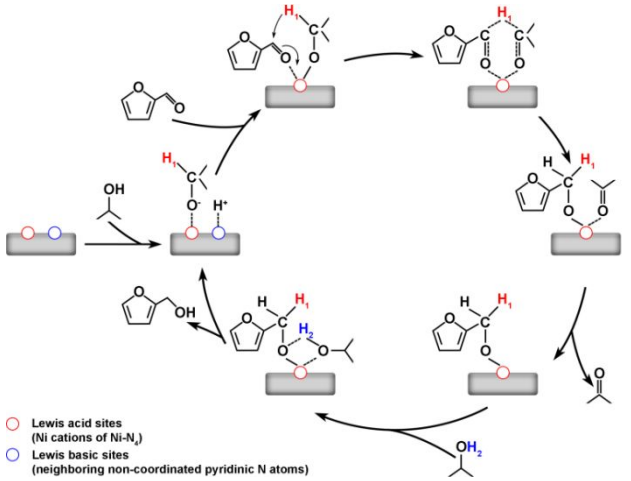

Figure 5. Possible reaction mechanism for catalytic transfer hydrogenation of FF.

In Figure 4b, the influence of reaction temperature to the hydrogenation of FF was investigated over Ni-SAs/NC using 2-ProOH as H-donor from 110-140 °C for 3 h. The FF conversion significantly increased from 64.1% at 110 °C to 95.6% at 130 °C, while the selectivity decreased from 97.4% to 96.8%. Notably, with the increase of reaction temperature, the etherification of FF and 2-ProOH to form isopropoxymethylfuran resulted in a decrease of selectivity of FAL. Further increase in reaction temperature e.g. 140 °C has no obvious effect on conversion. Figure 4c showed the effect of reaction time on the catalytic activity. Low conversion of 58.6% and 97.1% selectivity was obtained at 2 h. Selectivity decreased from 97.1% to 96.3% at the reaction time of 5 h. Obviously, prolongation of the reaction time can increase the conversion of FF, but the slight decrease in selectivity also occurs resulting from etherification between the FF and 2-ProOH.

3.3.3. Reaction Kinetics Study

The reaction was conducted at three different reaction temperatures of 100, 110, and 120 °C to study kinetic behaviors of the CTH of FF to FAL. Since the amount of catalyst is fixed and 2-ProOH is excessive, we assumed that this reaction is a first-order reaction of the FF concentration function. Obviously, as shown in Figure 4d, ln (C_t/C_0) is linearly related to reaction time at different temperatures. The reaction rate constants (k) in this experiment were calculated to be 0.2489, 0.3026 and 0.4567 min^{-1} for the temperatures 100, 110, and 120 °C, respectively. According to the Arrhenius plot, the activation energy (E_a) was determined to be 36.86 kJ mol^{-1} over the Ni-SAs/NC catalyst for CTH of FF into FAL using 2-ProOH as hydrogen donor. This value is higher than FF adsorption energy, which shows that the reaction was controlled by surface dynamics.[51] Meanwhile, this E_a value is lower than the recently reported literatures for selective conversion of FF into FAL (Table S4). The low activation energy may be related to the chemical environment of the atom-dispersed Ni-N_4 structure. So, the catalytic activity of Ni-SAs/NC is higher than most catalysts in Table S4 under the mild conditions.

3.3.4. Reaction mechanism studies

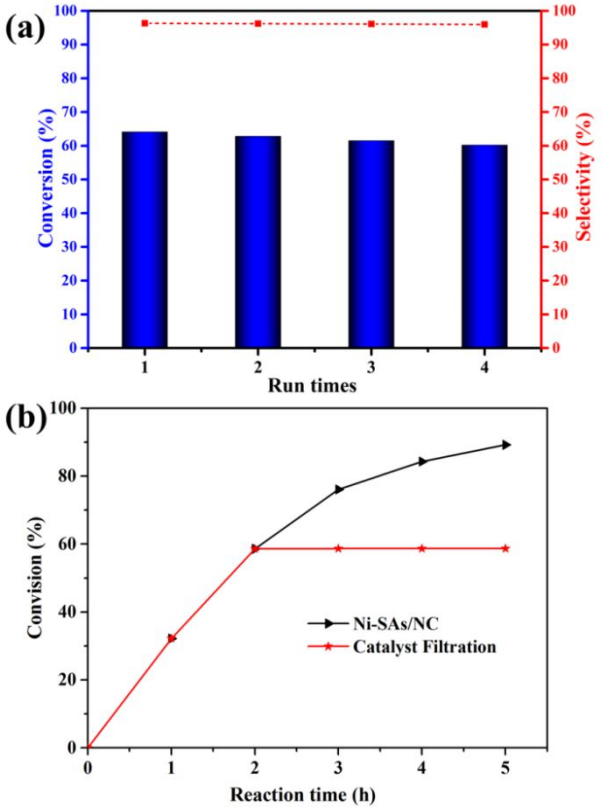

Figure 6. (a) Reusability of Ni-SAs/NC catalysts for the hydrogenation of furfural. Reaction conditions: 1 mmol FF, 8 mL 2-ProOH, 25mg catalyst, 110 °C, 3 h, 2 MPa N_2. (b) Metal leaching experiment with catalyst (black) and with filtrate (red).

According to previous reports, Lewis acid and basic sites of the catalyst are the main effective factors to make the catalytic transfer of hydrogenated carbonyl compounds.[52-53] The XANES test could prove that the Ni valence is 0 to +2 in the Ni-SAs/NC (Figure 2a), so Ni is considered to be Lewis acid site. In addition, XPS also proved that Ni-SAs/NC catalyst contains a large number of pyridine-N, which created Lewis base sites.[54] To verify the frustrated Lewis pairs (FLP) mechanism, we conducted two controlled experiments. When the formic acid was added as Lewis acid in the FF hydrogenation reaction, it was found that the conversion rate dropped sharply from 85.1% to 3.7%, and the selectivity completely dropped to 0. Then we

added potassium thiocyanate (KSCN) to poison the Ni (Lewis acid sites), and the conversion rate decreased to 3.0% without any formation of FAL. The above results indicate that Lewis acid base position is necessary for hydrogenation reaction. In combination with relevant literature,[14, 18, 23, 25] a mechanism for FF transfer hydrogenation catalyzed by Ni-SAs/NC catalyst was proposed (Figure 5). First, 2-ProOH adsorbed on the surface of the Ni-SAs/NC catalyst interacts with the acid-base sites (Ni cations and neighboring non-coordinated pyridinic N) on the catalyst surface, resulting in 2-ProOH dissociation forming the corresponding Ni bound isopropoxide and N-H^+.[25] At the same time, the carbonyl group of FF is also adsorbed and activated by the Lewis acid sites (Ni cations). Subsequently, a six-membered ring transition state forms through the coordination between the Ni bound isopropoxide and the activated carbonyl group, and the β-H of Ni bound isopropoxide is directly transferred to the carbonyl group of FF,[18] meanwhile the acetone forms and then releases. Finally, the formation of FF can easily be obtained through proton transfer from another 2-ProOH to deprotonated FF along the hydrogen bonding, in which the transition state has a four membered-ring.[14]

Table 2. Catalytic transfer hydrogenation of Various Carbonyl Compounds over Ni-SAs/NC.[a]

Entry	Substrate	Product	Temp (°C)	Time (h)	Conv. (%)	Sel. (%)	TOF [b] (h^{-1})
1	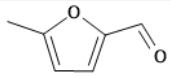	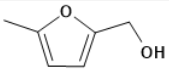	140	3	74.7	98.6	243
2	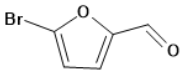	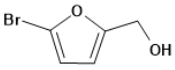	140	3	56.3	98.3	183
3	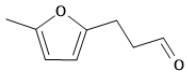	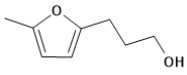	140	3	48.6	98.9	158
4	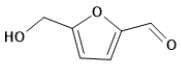	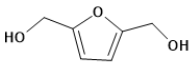	180	3	22.6	96.5	74
5	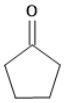	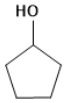	160	3	74.5	100	242
6	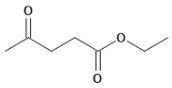	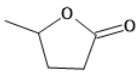	180	3	81.8	63.9	266
7	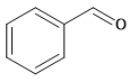	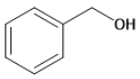	140	4	93.2	100	228
8	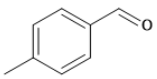	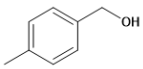	140	4	51.6	100	126
9	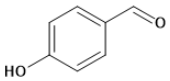	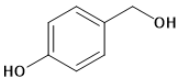	170	3	29.6	100	96

[a] Reaction conditions: 0.5 mmol substrate, 25mg catalyst, 8mL 2-ProOH, 2 MPa N_2. [b] TOF = (moles of substrate)/(moles of "Ni" × time).

3.3.5. Catalysts Stability

In Figure 6a, the activity and selectivity of Ni-SAs/NC were not significantly reduced when the catalyst has been used for 4 cycles. The high catalytic stability is attributed to the stable Ni-N_4 structure formed by N-doped carbon, which plays an important role in preventing metal atoms from reunion. The XRD results show that the characteristic peaks of the used

catalyst and the fresh catalyst have not changed, and no characteristic peaks of Ni appear (Figure S12). Moreover, the Ni atoms did not agglomerate and remained atomically dispersed according to the AC-TEM (Figure S13). In addition, leaching experiments were conducted to further verify the stability of the Ni-SAs/NC in Figure 6b. After filtration, the reaction of the solution basically stopped at a conversion rate of 58.6%, and Ni was not observed as a detectable limit of ICP-OES in the filtrate after the reaction, indicating that the Ni metal was not leachable. It is also proved that the Ni-SAs/NC catalyst is heterogeneous and stable.

3.3.6. Substrate Scope

The excellent catalytic activity of Ni-SAs/NC has been discussed in CTH of FF. The range of various substrates was also tested, including other biomass-derived carbonyl compounds, and representative other α,β-unsaturated aldehydes (Table 2). The analysis showed that Ni-SAs/NC demonstrated high TOF for a variety of substrates, which minimum TOF is 74 h^{-1} for 5-hydroxymethylfurfural (Entry 4). When a methyl, Br and hydroxymethyl were introduced in FF, significantly lower conversion rates and TOF were found (Entry 1-4). This is due to the electron-donating nature of the group increasing the electron density on the carbonyl C atom, and this situation is not conducive to activating the carbonyl carbon.[46] In addition, the presence of steric hindrance also affects the activation of the carbonyl group. Similarly, the introduction of other groups on benzaldehyde also reduces the catalytic activity (Entry 7-9). In general, these results indicated that Ni-SAs/NC showed high selectivity and excellent TOF, and have great potential applications in the efficient conversion of α,β-unsaturated aldehydes through environmentally friendly CTH reaction.

4. Conclusions

Single-atom catalyst Ni-SAs/NC was successfully prepared and well demonstrated through various advanced microscopy techniques, XAFS confirmed that Ni-N_4 coordination structure of the Ni-SAs/NC. Ni-SAs/NC showed a high performance for CTH of FF to FAL with TOF as high as 832 h^{-1} and selectivity as high as 97.1%. Factors influencing the reaction, including H-donor solvent, temperature and reaction time were discussed in detail. Ni-SAs/NC also exhibited good stability and no significantly decrease in catalytic activity after four cycles. The main reason for the high activity and stability of the Ni-SAs/NC is the clear atom-dispersed Ni-N_4 structure for CTH of FF to FAL. Moreover, Ni-SAs/NC could also efficiently transform the other α,β-unsaturated aldehydes to the corresponding alcohol in the substrate expansion test. Our efficient and stable single-atoms Ni catalyst presents a novel strategy for the CTH of biomass compounds.

Conflicts of interest

The authors declare no competing financial interest.

Acknowledgements

This work was supported by the National Natural Science Foundation of China (No.31760190, 21531003, 21501024, 21971035), Special project of agricultural basic research in Yunnan (No.2017FG001026, 2017FG001055), Jilin Scientific and Technological Development Program (20170101198JC, 20190103017JH), Jilin Education Office (JJKH20180015KJ). Key Laboratory of State Forestry Adminstration for Highly-Efficient Utilization of Forestry Biomass Resources in Southwest China (2019-KF06).

Notes and references

1 L. T. Mika, E. Csefalvay and A. Nemeth, *Chem. Rev.*, 2018, **118**, 505-613.
2 G. Bagnato, A. Figoli, C. Ursino, F. Galiano and A. Sanna, *J. Mater. Chem. A,* 2018, **6**, 4955-4965.
3 S. Gyergyek, A. Kocjan, M. Grilc, B. Likozar, B. Hoevar and D. Makovec, *Green Chem.,* 2020, **22**, 5978-5983.
4 R. Fang, A. Dhakshinamoorthy, Y. Li and H. Garcia, *Chem. Soc. Rev.*, 2020, **49**, 3638-3687.
5 X. Lan and T. Wang, *ACS Catal.*, 2020, **10**, 2764-2790.
6 R. Mariscal, P. Maireles-Torres, M. Ojeda, I. Sádaba and M. López Granados, *Energy Environ. Sci.,* 2016, **9**, 1144-1189.
7 S. Chen, R. Wojcieszak, F. Dumeignil, E. Marceau and S. Royer, *Chem. Rev.,* 2018, **118**, 11023-11117.
8 M. J. Islam, M. Granollers Mesa, A. Osatiashtiani, M. J. Taylor, J. C. Manayil, C. M. A. Parlett, M. A. Isaacs and G. Kyriakou, *Appl. Catal., B,* 2020, **273**, 119062-119075.
9 H. Li, J. He, A. Riisager, S. Saravanamurugan, B. Song and S. Yang, *ACS Catal.*, 2016, **6**, 7722-7727.
10 P. N. Paulino, R. F. Perez, N. G. Figueiredo and M. A. Fraga, *Green Chem.*, 2017, **19**, 3759-3763.
11 S. Zhou, F. Dai, Z. Xiang, T. Song, D. Liu, F. Lu and H. Qi, *Appl. Catal., B,* 2019, **248**, 31-43.
12 W. Luo, W. Cao, P. C. A. Bruijnincx, L. Lin, A. Wang and T. Zhang, *Green Chem.*, 2019, **21**, 3744-3768.
13 T. A. Bender, J. A. Dabrowski and M. R. Gagné, *Nat Rev Chem.*, 2018, **2**, 35-46.
14 W. Gong, C. Chen, Y. Zhang, H. Zhou, H. Wang, H. Zhang, Y. Zhang, G. Wang and H. Zhao, *ACS Sustainable Chem. Eng.,* 2017, **5**, 2172-2180.
15 Z. Pan, H. Jiang, B. Gong, R. Luo, W. Zhang and G. Wang, *J. Mater. Chem. A,* 2020, **8**, 23376-23384.
16 R. A. Farrar-Tobar, A. Dell'Acqua, S. Tin and J. G. de Vries, *Green Chem.*, 2020, **22**, 3323-3357.
17 M. Ma, H. Liu, J. Cao, P. Hou, J. Huang, X. Xu, H. Yue, G. Tian and S. Feng, *Mol. Catal,* 2019, **467**, 52-60.
18 A. H. Valekar, M. Lee, J. W. Yoon, J. Kwak, D.-Y. Hong, K.-R. Oh, G.-Y. Cha, Y.-U. Kwon, J. Jung, J.-S. Chang and Y. K. Hwang, *ACS Catal.*, 2020, **10**, 3720-3732.
19 S. Zhou, G. Chen, X. Feng, M. Wang, T. Song, D. Liu, F. Lu and H. Qi, *Green Chem.*, 2018, **20**, 3593-3603.
20 J. Du, J. Zhang, Y. Sun, W. Jia, Z. Si, H. Gao, X. Tang, X. Zeng, T. Lei, S. Liu and L. Lin, *J. Catal.*, 2018, **368**, 69-78.
21 M. J. Taylor, L. J. Durndell, M. A. Isaacs, C. M. A. Parlett, K. Wilson, A. F. Lee and G. Kyriakou, *Appl. Catal., B,* 2016, **180**, 580-585.
22 P. Panagiotopoulou, N. Martin and D. G. Vlachos, *ChemSusChem*, 2015, **8**, 2046-2054.
23 J. He, L. Schill, S. Yang and A. Riisager, *ACS Sustainable Chem. Eng.,* 2018, **6**, 17220-17229.
24 J. Wu, G. Gao, J. Li, P. Sun, X. Long and F. Li, *Appl. Catal., B,* 2017, **203**, 227-236.

25 W. Liu, Y. Chen, H. Qi, L. Zhang, W. Yan, X. Liu, X. Yang, S. Miao, W. Wang, C. Liu, A. Wang, J. Li and T. Zhang, *Angew. Chem., Int. Ed.,* 2018, **57**, 7071-7075.
26 X. Hai, X. Zhao, N. Guo, C. Yao, C. Chen, W. Liu, Y. Du, H. Yan, J. Li, Z. Chen, X. Li, Z. Li, H. Xu, P. Lyu, J. Zhang, M. Lin, C. Su, S. J. Pennycook, C. Zhang, S. Xi and J. Lu, *ACS Catal.*, 2020, **10**, 5862-5870.
27 Y.-S. Wei, M. Zhang, R. Zou and Q. Xu, *Chem. Rev.*, 2020, **120**, 12089−12174.
28 M. Chen, X. Li, F. Yang, B. Li, T. Stracensky, S. Karakalos, S. Mukerjee, Q. Jia, D. Su, G. Wang, G. Wu and H. Xu, *ACS Catal.*, 2020, **10**, 10523-10534.
29 Z. Li, S. Ji, Y. Liu, X. Cao, S. Tian, Y. Chen, Z. Niu and Y. Li, *Chem Rev.*, 2020, **120**, 623-682.
30 H. Huang, K. Shen, F. Chen and Y. Li, *ACS Catal.*, 2020, **10**, 6579-6586.
31 S. Gong, C. Wang, P. Jiang, L. Hu, H. Lei and Q. Chen, *J. Mater. Chem. A,* 2018, **6**, 13254-13262.
32 Y. Deng, B. Chi, X. Tian, Z. Cui, E. Liu, Q. Jia, W. Fan, G. Wang, D. Dang, M. Li, K. Zang, J. Luo, Y. Hu, S. Liao, X. Sun and S. Mukerjee, *J. Mater. Chem. A,* 2019, **7**, 5020-5030.
33 Q. Zhang, Z. Duan, Y. Wang, L. Li, B. Nan and J. Guan, *J. Mater. Chem. A,* 2020, **8**, 19665-19673.
34 C. Gao, J. Low, R. Long, T. Kong, J. Zhu and Y. Xiong, *Chem Rev.*, 2020, **120**, 12175–12216.
35 H. Zhou, S. Hong, H. Zhang, Y. Chen, H. Xu, X. Wang, Z. Jiang, S. Chen and Y. Liu, *Appl. Catal., B,* 2019, **256**, 117767-117777.
36 Y. Xiong, J. Dong, Z. Q. Huang, P. Xin, W. Chen, Y. Wang, Z. Li, Z. Jin, W. Xing, Z. Zhuang, J. Ye, X. Wei, R. Cao, L. Gu, S. Sun, L. Zhuang, X. Chen, H. Yang, C. Chen, Q. Peng, C. R. Chang, D. Wang and Y. Li, *Nature Nanotechnol,* 2020, **15**, 390-397.
37 X. Wang, Z. Chen, X. Zhao, T. Yao, W. Chen, R. You, C. Zhao, G. Wu, J. Wang, W. Huang, J. Yang, X. Hong, S. Wei, Y. Wu and Y. Li, *Angew. Chem., Int. Ed.,* 2018, **57**, 1944-1948.
38 Q. Wang, Y. Ji, Y. Lei, Y. Wang, Y. Wang, Y. Li and S. Wang, *ACS Energy Lett.*, 2018, **3**, 1183-1191.
39 Y.-j. Wu, X.-h. Wu, T.-x. Tu, P.-f. Zhang, J.-t. Li, Y. Zhou, L. Huang and S.-g. Sun, *Appl. Catal., B,* 2020, **278**, 119259-119271.
40 J. Yang, D. Zeng, J. Li, L. Dong, W.-J. Ong and Y. He, *Chem. Eng. J.,* 2021, **404**, 126376-126387.
41 Y. Fan, S. Li, Y. Wang, C. Zhuang, X. Liu, G. Zhu and X. Zou, *Nanoscale*, 2020, **12**, 18296-18304.
42 H. Shang, Z. Jiang, D. Zhou, J. Pei, Y. Wang, J. Dong, X. Zheng, J. Zhang and W. Chen, *Chem Sci.*, 2020, **11**, 5994-5999.
43 Y. He, Y. Li, J. Zhang, S. Wang, D. Huang, G. Yang, X. Yi, H. Lin, X. Han, W. Hu, Y. Deng and J. Ye, *Nano Energy*, 2020, 77, 105010-105018.
44 L. Zhang, N. Shang, S. Gao, J. Wang, T. Meng, C. Du, T. Shen, J. Huang, Q. Wu, H. Wang, Y. Qiao, C. Wang, Y. Gao and Z. Wang, *ACS Catal.*, 2020, **10**, 8672-8682.
45 C. F. Wen, F. Mao, Y. Liu, X. Y. Zhang, H. Q. Fu, L. R. Zheng, P. F. Liu and H. G. Yang, *ACS Catal.*, 2019, **10**, 1086-1093.
46 G. Huang, L. Yang, X. Ma, J. Jiang, S.H. Yu, H.L. Jiang, *Chem. Eur. J.* 2016, **22**, 3470-3477.
47 H. Su, P. Gao, M. Y. Wang, G. Y. Zhai, J. J. Zhang, T. J. Zhao, J. Su, M. Antonietti, X. H. Li and J. S. Chen, *Angew. Chem., Int. Ed.,* 2018, **57**, 15194-15198.
48 X. Dai, Z. Chen, T. Yao, L. Zheng, Y. Lin, W. Liu, H. Ju, J. Zhu, X. Hong, S. Wei, Y. Wu and Y. Li, *Chem. Commun.,* 2017, **53**, 11568-11571.
49 J. He, M. R. Nielsen, T. W. Hansen, S. Yang and A. Riisager, *Catal. Sci. Technol*, 2019, **9**, 1289-1300.
50 M. Ma, P. Hou, J. Cao, H. Liu, X. Yan, X. Xu, H. Yue, G. Tian and S. Feng, *Green Chem.*, 2019, **21**, 5969-5979.
51 K. Chen, J.-L.L, C-D Wu, *Angew. Chem., Int. Ed,* 2020, **132**, 1941-1947.
52 Y. Shao, K. Sun, Q. Li, Q. Liu, S. Zhang, Q. Liu, G. Hu and X. Hu, *Green Chem.*, 2019, **21**, 4499-4511.
53 F. Li, L.J. France, Z. Cai, Y. Li, S. Liu, H. Lou, J. Long, X. Li, *Appl. Catal., B,* 2020, **279,** 119389-119401.
54 D. Guo, R. Shibuya, C. Akiba, S. Saji, T. Kondo, J. Nakamura, *Science,* 2016, **351**, 361-365.

Graphical Abstract:

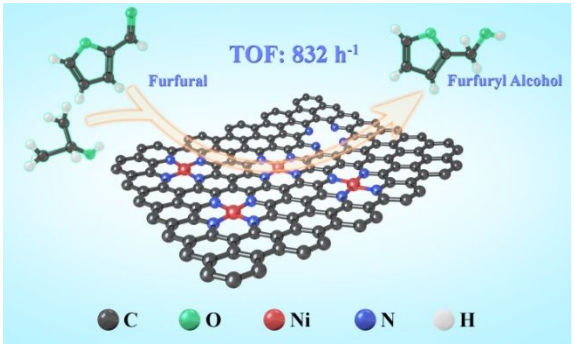

Single-atoms Ni catalyst is first utilized in the catalytic transfer hydrogenation of furfural to furfuryl alcohol.